Chemical Engineering Journal 154 (2009) 174–184

Contents lists available at ScienceDirect

Chemical Engineering Journal

journal homepage: www.elsevier.com/locate/cej

# Evaluation of kinetic models for the partial oxidation of methane to synthesis gas over a Pt/PrCeZrO$_x$ catalyst coated on a triangular monolith

Elena L. Gubanova[a,b], Yves Schuurman[a], Vladislav A. Sadykov[b], Claude Mirodatos[a], Andre C. van Veen[a,c,*]

[a] Institut de Recherches sur la Catalyse et l'Environnement de LYON, UMR 5256 (CNRS - Université Claude Bernard Lyon 1), 2 avenue Albert Einstein, 69626 Villeurbanne Cédex, France
[b] Boreskov Institute of Catalysis SB RAS, Pr. Lavrientieva, 5, 630090 Novosibirsk, Russia
[c] Ruhr-University Bochum, Lehrstuhl für Technische Chemie, Office NC 5/69, Universitätsstraße 150, D-44801 Bochum, Germany

ARTICLE INFO

*Article history:*
Received 15 December 2008
Received in revised form 10 March 2009
Accepted 21 May 2009

*Keywords:*
Kinetic model
Reaction mechanism
Platinum
Fluorite structured support
Oxygen storage material

ABSTRACT

The evaluation of kinetic models for the partial oxidation of methane to synthesis gas over a 1.4-wt% Pt/Pr$_{0.3}$Ce$_{0.35}$Zr$_{0.35}$O$_x$ catalyst coated on the surface of a triangular corundum channel is presented. The mathematical form of the tested models accounts for global surface steps. The formulation of reaction steps for two cases proposed in the literature contained lumped formulations to restrict reasonably the number of parameters to estimate. One mechanism considering an oxygen assisted methane activation and another considering methane dissociation without oxygen involvement were tested. In both cases a satisfying description of the experimental data was possible, suggesting that the initial activation of methane is of less importance for the overall progress of the partial oxidation than the oxidation of carbonaceous intermediates to adsorbed carbon monoxide assumed in both cases. Comparing the kinetics over unsupported platinum extensively reported in literature to the data over the 1.4-wt% Pt/Pr$_{0.3}$Ce$_{0.35}$Zr$_{0.35}$O$_x$ catalyst in this work reveals significantly different rates for oxygen adsorption and carbon monoxide oxidation. These differences are explained by considering the active role the ceria plays in the catalyst performance.



## 1. Introduction

Methane is the main component of natural gas, being forecasted to outlast crude oil by a significant time span (around 60 years) [1]. Nevertheless, the gas industry is currently in a relatively underdeveloped state. Furthermore, natural gas is abundant in many locations around the world [2]. Currently, the use of natural gas as feedstock for chemical or fuels synthesis is regaining significant interest due to the recent rise in supply costs for oil. This marks a major reversal of the recent past situation where the use of gas for chemical synthesis was considered uneconomical because of high costs of natural gas storage and transportation from the remote reservoirs where it is most abundant. Methods to enhance the value of natural gas, either by synthesizing more valuable chemicals or more readily transportable products, have been investigated, particularly in the last 20 years, but yields tended to be too low to compete with oil caused by selectivity issues during methane activation where the added value products are more reactive than methane as reactant.

As a direct use of methane for producing chemicals, e.g. by the oxidative coupling, remains still in the research stage, the technically most advanced process route passes via synthesis gas. The generation of synthesis gas might involve the strongly endothermic steam reforming, the autothermal reforming or the partial oxidation of methane to synthesis gas. Aiming on efficient and compact reactors, the partial oxidation of methane is the most attractive option as this reaction shows the highest reaction rates. Nevertheless, this reaction is difficult to control, especially when the reaction should proceed at elevated pressures. Structured reactors, such as monoliths, can improve the control of the reaction as these configurations improve the mass transfer between the gas and the catalyst phase and the flame arrestor capability of confined structures allows a reasonable safe operation. On the other hand, suitable coated catalysts need to be developed and optimized. A second urgent need for designing a synthesis gas generator is the knowledge of the kinetics for the partial oxidation of methane over the developed catalyst, due to its wide range applicability under steep gradients preferably using a microkinetic model or at least a kinetic model considering more global surface reaction steps. This implies however that the reaction scheme should be explored. Generally,

* Corresponding author at: Ruhr-University Bochum, Lehrstuhl für Technische Chemie, Office NC 5/69, Universitätsstraße 150, D-44780 Bochum, Germany. Tel.: +49 234 32 24217; fax: +49 234 32 14182.
*E-mail address:* andre.vanveen@rub.de (A.C. van Veen).

1385-8947/$ – see front matter © 2009 Elsevier B.V. All rights reserved.
doi:10.1016/j.cej.2009.05.038

**Nomenclature**

| | |
|---|---|
| $C_j$ | molar concentration of species $j$ (mol/m$^3_f$) |
| $d_h$ | hydraulic diameter (m) |
| $d_i$ | internal side of triangular monolith (m) |
| $D$ | molecular diffusion coefficient (m$^2$/s) |
| $Da$ | Damköhler number, $Da = r_j \delta_{wash} d_h / 4 C_j D$ |
| $E_{act}$ | activation energy (J/mol) |
| $F_j$ | molar flow rate of species $j$ (mol/s) |
| $k_j$ | mass transfer coefficient from gas to solid interface for species $j$ (m$^3_f$/m$^2_s$ s) |
| $L$ | reactor length (m) |
| $Pr$ | Prandtl number, $Pr = C_p \mu / \lambda_e$ |
| $R$ | gas constant (J/mol K) |
| $R_j$ | rate of disappearance of component $j$ (mol/m$^2_{cat}$ s) |
| $R$ | overall reaction rate |
| $Re$ | Reynolds number, $Re = \rho u d_h / \mu$ |
| $Sc$ | Schmidt number, $Sc = \mu / \rho D$ |
| $Sh$ | Sherwood number, $Sh = k_g d_h / D$ |
| $T$ | temperature (K) |
| $u$ | gas velocity (m/s) |
| $V$ | reactor volume (m$^3_r$) |
| $W$ | catalyst mass (kg) |
| $X_{CH_4}$ | $CH_4$ conversion |
| $z$ | distance inside the monolith (m) |
| $\delta_{wash}$ | thickness of the washcoat (m$_s$) |
| $\Delta H_R$ | enthalpy of reaction (J/mol) |
| $\Delta S_R$ | entropy of reaction (J/mol K) |
| $\lambda_e$ | effective thermal conductivity of the solid phase (J/m s K) |
| $\mu$ | viscosity of the gas mixture (Pa s) |
| $\rho$ | density of the gas mixture (kg/m$^3_f$) |
| $\rho_s$ | catalyst density (kg/m$^3_s$) |

*Superscripts*

| | |
|---|---|
| 0 | inlet |
| p | inside solid phase washcoat or particle |
| s | surface |

*Subscripts*

| | |
|---|---|
| $j$ | component or species |
| f | fluid phase |
| r | reactor |
| s | solid phase |

the literature reports of two distinct mechanisms for explaining the formation of syngas.

The indirect pathway postulates that $CH_4$ is first totally oxidized to $CO_2$ and $H_2O$ (in a strongly exothermic reaction) and then reformed to produce syngas (by strongly endothermic reactions). One major proof of the existence of such an exothermic–endothermic sequence has been the observation of sharp hot spots at the entrance of the reactor, which can cause detrimental effects on the stability of the catalytic material and can cause severe heat transport limitations [3]. The direct pathway postulates the formation of $H_2$ and CO as primary products, eventually further oxidized into $CO_2$ and $H_2O$, depending on process conditions (contact time, O/C ratios, etc.). The main evidence in favor of a direct path is the observation of syngas at extremely short contact times, in the presence of unreacted oxygen [4].

Despite of the fact that there is extensive research on the mechanism of the CPOM over Pt and even detailed microkinetic studies have been published recently [5], catalyst stability is a major issue under the severe operating conditions. One way to achieve stable Pt-based catalysts is the option to support Pt not on an inert carrier, but to employ supports with oxygen storage capacity as demonstrated in our recent work [6]. In fact, even more efficient in preventing coking than La-doped systems described in the latter work are Pr or Gd-doped materials investigated in this work. Nevertheless, the increased catalyst stability comes at the price that the catalyst can no longer be simply considered as a Pt system, but that the active support might have a pronounced impact on the reaction mechanism possibly even turning the catalyst into a bi-functional system. Obviously, kinetic information on simple Pt catalysts can serve as starting information, but there is a need to investigate the mechanistic features [7] and the kinetics over new catalysts.

However, the fast rate at which the CPOM reaction is proceeding makes mass transport limitations likely to occur, thus masking the intrinsic catalyst performance. In order to minimize mass transfer limitations several experimental reactor configurations have been used to study the reaction kinetics of the CPOM at short residence times and high temperatures. These configurations have in common that they employ the catalytic material in a structured configuration being in contrast to fixed beds used in conventional reactors. A catalytic annular reactor was applied by Beretta et al. [8] to study the intrinsic kinetics of the CPO reaction. In the presence of heat-transport limitations, de Smet et al. [9] developed an experimental reactor, containing a single Pt gauze as catalyst. Heat-transport limitations were first explicitly taken into account and later experimentally quantified by measuring the catalyst temperature with a spot-welded thermocouple attached to the Pt gauze. It was demonstrated that experiments could not be performed at conditions where both conversion and selectivities are determined by chemical phenomena alone. Moreover, taking into account the relevant transport phenomena, de Smet et al. [9] developed a reactor model to obtain the intrinsic kinetic parameters of the CPOM reaction on the Pt gauze.

The present work reports on the development of a kinetic model for the catalytic partial oxidation of methane over a single monolith channel in the presence of unavoidable transport phenomena. Experimental data used for mathematical modeling will be presented as dot symbols along the results of the modeling depicted as lines. Experiments were performed studying the influence of the catalyst temperature, the reactant space-time and the inlet $CH_4/O_2$ ratio. The relative importance of dry reforming was studied as well. The aim of present study is to provide a comprehensive kinetic mechanism that can account for synthesis gas production and that can give insights into the role of the support on the catalytic performance.

## 2. Experimental

The preparation of the fluorite structured support material and impregnation of Pt by an incipient wetness technique was already reported in an earlier work [6]. Briefly, aqueous solutions of starting salts (nitrates of Ce and Pr), oxychloride of zirconium, citric acid (CA), ethylene glycol (EG), ethylene diamine (ED) were employed in a molar ratio of CA:EG:ED:Me(Pr + Ce + Zr) = 3.75:11.25:3.75:1 for preparing the $Pr_{0.3}Ce_{0.35}Zr_{0.35}O_x$ complex oxide support. Ethylene glycol and citric acid were used as complex formation reagents, ethylene diamine was chosen as additional complex builder. Citric acid was dissolved in ethylene glycol at a ratio of CA:EG = 1:3 at 60 °C. At the same time, aqueous nitrates of Ce ($Ce(NO_3)_3{\cdot}6H_2O$) and Pr ($Pr(NO_3)_3{\cdot}6H_2O$) were dissolved in 30 ml of distilled water adding the $ZrOCl_2$ solution thereafter. Both solutions were mixed and kept at 50 °C during 72 h for removing the solvent entirely. The product was further calcined for 4 h in air at 500 °C.

Single channel substrates catalysts were cut from an $\alpha$-$Al_2O_3$ monolith with triangular channels. The wall thickness was 0.2 mm,

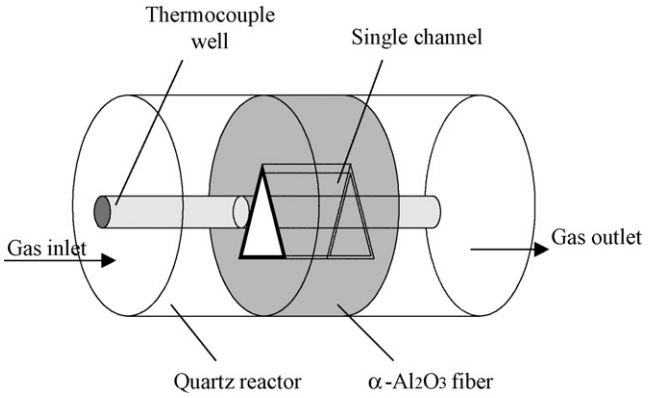


**Fig. 1.** Scheme of the quartz reactor charged with a single monolithic channel.

the side width of the inside triangle amounted to 2.33 mm and the channel length was cut to 10 mm. After annealing at 1300 °C the specific surface area of the corundum support was estimated to be 3 $m^2$/g. Layers of $Pr_{0.3}Ce_{0.35}Zr_{0.35}O_x$ were supported on these substrates by washcoating ultrasonically homogenized water based suspensions of 5 g ceria–zirconia mixed oxide dispersed in 60 ml of distilled water. Adjusting the pH value to 3 and increasing the viscosity of the suspension was accomplished by the addition of nitric acid and polyethylene glycol, respectively.

Pt deposition involved a $H_2PtCl_6$ solution and dropwise incipient wetness impregnation adapted to channel substrates to resemble as close as possible the preparation of powdered catalysts. The impregnation of the active phase was followed by drying and calcination at 900 °C in air.

The kinetic tests were performed over a 1.4-wt% $Pt/Pr_{0.3}Ce_{0.35}Zr_{0.35}O_x/\alpha\text{-}Al_2O_3$ single channel of 10 mm length in a plug-flow reactor (schematic depicted in Fig. 1) in an entirely computer controlled test bench. A preheater with individual control loop was fitted to the system directly upstream of the reactor. The gas supply was either ensured by a central gas supply system ($H_2$, $O_2$, $N_2$), or by individual gas tanks (Ar, $CH_4$, $CO_2$, He). Aiming at experiments with shorter contact time, the entire feeding section is made from 1/4″ stainless steel tubes (external diameter of 6.3 mm) and assembled with Swagelok type fittings to avoid excessive pressure drops at the required high flow rates. Flows were adjusted using calibrated Brooks 5850 TR mass flow controllers and gases were distributed in two distinct gas lines for pretreatment and reaction that could be switched over by 1/4″ valco valves with electric actuators.

All experiments were performed at atmospheric pressure. A typical run consisted of varying the oven temperature from 700 up to 850 °C, with 1 h dwell steps at temperature increments of 25–50 °C. At each temperature, conversions and selectivities were estimated from repeated analysis once stable values were measured. Typically the catalyst showed stable operation once an induction period of 20 min was passed and performance data could be averaged over the remaining 40 min. Nevertheless, prior to kinetic investigations, the catalyst underwent a standard conditioning procedure consisting of repeated runs at a fixed low flow rate of 100 ml $min^{-1}$, feeding a diluted gas mixture with a composition of 7 vol.% $CH_4$, a $O_2/CH_4$ ratio of 0.5 in $N_2$ added to balance. The catalyst conditioning was complete when stable performances were reached at each temperature in the whole range. To operate far from thermodynamic control, kinetic experiments were performed at higher values of flow rates than the conditioning one. Table 1 summarizes the range of experimental conditions investigated.

**Table 1**
Experimental conditions of kinetic experiments.

| Varied parameter and range | Feed: 6.6%$CH_4$ + 3.3%$O_2$ ($N_2$-balance) |
|---|---|
| Oven temperature/°C | 700–850 |
| Flow rate/ml/min | 400–1400 |
| $CH_4/O_2$ | 2–4.5 |
| Concentration $CO_2$ added in the feed/% | 0–4 |

The influent and effluent analysis made use of a μ-GC having 2 analytical modules (Agilent Micro-GC 300) delivering quantitative results on the sample gas composition in less than 160 s. Module 1 accomplishing the detection of $H_2$, $O_2$, $N_2$, $CH_4$ and CO was a molecular sieve 5 Å/10 m with Ar as carrier gas (slightly lower sensitivity but reasonable linearity for the hydrogen response) and a backflush system preventing an accumulation of strongly interacting compounds like water, $CO_2$ and higher hydrocarbons on the column. Module 2 operated a PoraPLOT Q 8 m with He as carrier gas and detected next to an unexploited mixed peak of permanent gases $CH_4$ and $CO_2$. The amount of water in the sample was not directly detected but taken as average of the well matching values calculated from the hydrogen and oxygen element balances.

## 3. Modeling approach

### 3.1. 1D mathematical reactor model

A one-dimensional heterogeneous model accounting for the interfacial concentration gradients has been used for the analysis of the experimental results [10]. The radial temperature gradients were not calculated, as the outside wall temperature was measured with a thermocouple (Fig. 1) and it was assumed that this corresponds to the actual catalyst temperature. The axial profile was also

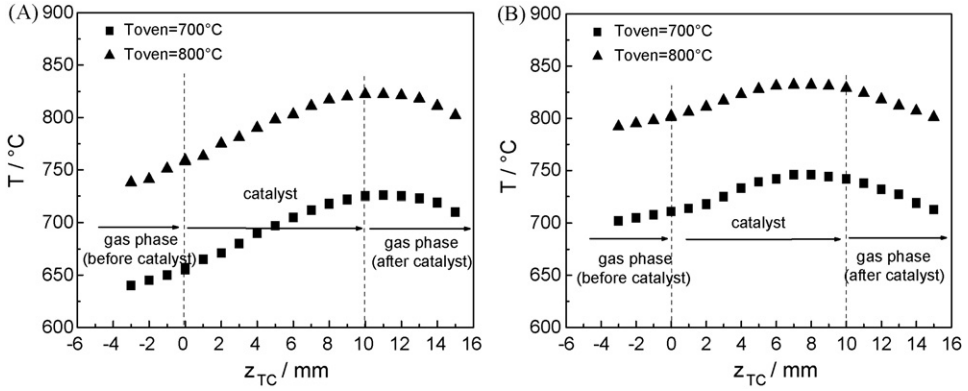


**Fig. 2.** Temperature profile of a 1.4-wt.% $Pt/Pr_{0.3}Ce_{0.35}Zr_{0.35}O_x$ channel without preheater (A) and with preheater at $T$ = 725 °C (B). Flow rate: 750 ml/min, channel length: 10 mm at 700 °C and 800 °C. Feed composition: 6.6%$CH_4$ + 3.3%$O_2$ ($N_2$-balance).

**Table 2**
Model equations.

| | |
|---|---|
| $\frac{dF_j}{dz} = 3d_i R_j \quad \text{mol/s m}_r$ | (1) |
| $R_j = k_{g,j}(C_j - C_j^s) \quad \text{mol/s m}^2_{cat}$ | (2) |
| *Initial conditions* | |
| $z = 0, \quad C_j = C_j^0$ | (3) |

**Table 3**
Mass transfer correlations for a triangular monolith channel.

| | |
|---|---|
| $2Sh = Sh_H - Da\frac{Sh_H}{Sh_T} + \sqrt{\left(\left(Sh_H - Da\frac{Sh_H}{Sh_T}\right)^2 + 4DaSh_H\right)}$ | (4) |
| $Sh_H = 1.89 + 8.933\left(\frac{1000}{l*}\right)^{-0.5386}\exp\left(-\frac{6.7275}{l*}\right)$ | (5) |
| $Sh_T = 2.47 + 6.854\left(\frac{1000}{l*}\right)^{-0.5174}\exp\left(-\frac{42.49}{l*}\right)$ | (6) |
| $l* = Re\,Sc\,\frac{d_h}{l}$ | (7) |

measured and is shown in Fig. 2. By applying high flow rates and a suitable preheating of the reactant stream controlled independently from the oven temperature, rather isothermal conditions are obtained. Axial dispersion in the monolith channel operated in the laminar flow regime can be neglected due to the very high superficial velocities applied in these experiments [11]. The one-dimensional heterogeneous model is used to simulate a single monolith channel.

Adopting the above hypotheses leads to the mathematical equations reported in the following Table 2. The coefficients for mass transfer in the monolith reactor are calculated according to the relations proposed by Groppi et al. [12,13]. The correlations for mass transfer are given in Table 3. The Sherwood number $Sh_T$ is the Sh number for constant wall temperature, $Sh_H$ refers to a constant wall heat flux. The actual Sh number is calculated using the interpolation formula of Brauer and Fetting [14], rearranged into (Eq. (4)). The density of the mixture has been calculated according to the law for ideal gases. Due to the small flow resistance of monoliths the pressure drop over the reactor is negligible and therefore the momentum equation has not been taken into account. The binary molecular diffusion coefficients are calculated from the Füller–Schettler–Giddings relation [15] and then the Wilke equation is used to calculate the diffusivities of the mixture [15].

### 3.2. Solution procedure

The set of equations to be solved consists of ordinary non-linear first-order differential equations that form a set of initial value problem coupled to non-linear algebraic equations. It should be noted that the differential equations reflect the change in species concentrations, which can be accessed as stoichiometic coefficient (Tables 6a and b for the mechanisms reported in Tables 5a and b, respecitvely) weighted linear combination of the reaction rates for the microkinetic steps considered. The set of differential algebraic equations (DAE) were numerically integrated using the ODEPACK library [16]. A number of physical properties and other variables (e.g. $\rho$, $u$, $\Delta H$) depend on the temperature, pressure or flow composition. These are updated after each integration step in a separate subroutine. All this is implemented in a FORTRAN code.

## 4. Results

### 4.1. Experimental results

In the range of conditions studied, CO, $CO_2$ and $H_2O$ were the main reaction products, while the selectivity to $H_2$ remained relatively low. The $H_2$ selectivity for all the applied conditions is plotted in Fig. 3 and shows an exponential increase with temperature. It becomes clear from Fig. 3 that the hydrogen selectivity was below 15% for the majority of conditions and reached peak values of 25%.

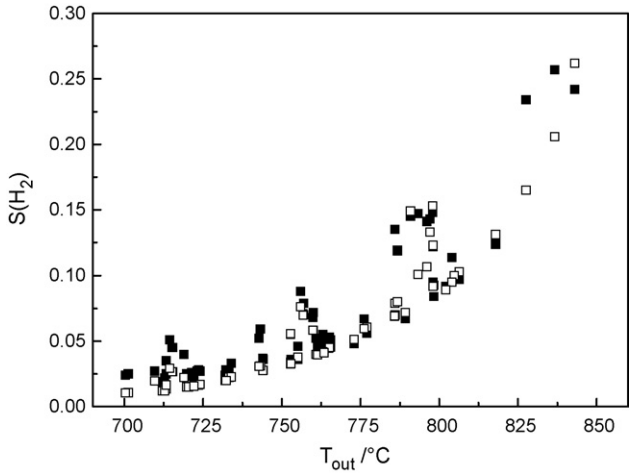


**Fig. 3.** Dependence of $H_2$ selectivity from temperature for the applied conditions. (Filled symbols indicate experimental data; open symbols show predictions by the kinetic model outlined in Table 5a and extended by step 6 to account for the hydrogen formation.)

### 4.2. Kinetic modeling

Several reaction mechanisms for the partial oxidation of methane over platinum based on elementary steps have been developed in the literature [4,5,9,17]. However, none of these take into account a possible role of the support in the catalyst performance. Therefore two models developed over platinum are evaluated for the data in this study in order to reveal the function of the support by comparing the values of the kinetic parameters.

Comparing coarsely the experimental results in this work to those reported in literature revealed large similarities with those used by de Smet et al. [17] in a modeling study. On the other hand, there is the major difference that de Smet et al. did not observe any hydrogen production over their Pt gauze catalyst at temperatures below 1000 °C preventing these authors to determine kinetic parameters for the hydrogen production. Nevertheless, the proposed kinetic scheme and kinetic parameters were considered highly suitable as a starting point for the kinetic description of the data in this work. The steps in the reaction model (mechanism) initially proposed by de Smet et al. [17] are summarized in Table 4.

All reaction steps were considered irreversible, except the sorption step 5 of carbon monoxide. Moreover, all reactions were considered to be first order in reactants and adsorbed species. Lacking experimental data the hydrogen production has been neglected as pointed out before. In fact these authors assumed even that the activation proceeds in an oxidative step leading immediately to the formation of water. The pre-exponential factor and the apparent

**Table 4**
Reaction mechanism proposed by de Smet et al. [17].

| Reaction | $A$ or $s^0$ ($Pa^{-1}\,s^{-1}$ or $s^{-1}$) | $E_{act}$ ($kJ\,mol^{-1}$) | Rate equation | Step |
|---|---|---|---|---|
| $O_{2,g} + 2^* \rightarrow 2O^*$ | 0.023 | 0 | $k_1 P_{O_2}\theta_*$ | 1 |
| $CH_{4,g} + 2O^* \rightarrow C^* + 2H_2O_g + *$ | $2.4 \times 10^5$ | 48.2 | $k_2 P_{CH_4}\theta_*\theta_O$ | 2 |
| $C^* + O^* \rightarrow CO^* + *$ | $1 \times 10^{13}$ | 62.8 | $k_3\theta_C\theta_O$ | 3 |
| $CO^* + O^* \rightarrow CO_{2,g} + 2^*$ | $1 \times 10^{13}$ | 100 | $k_4\theta_{CO}\theta_O$ | 4 |
| $CO^* \rightarrow CO_g + *$ | $1 \times 10^{13}$ | 126 | $k_5\theta_{CO}$ | 5a |
| $CO_g + * \rightarrow CO^*$ | 0.84 | 0 | $k_6 P_{CO}\theta_*$ | 5b |

* denotes a Pt active site, $k_x$ denotes the term $A_x \exp(-E_{act,x}/RT)$ or $s^0{}_x \exp(-E_{act,x}/RT)$, respectively.

**Table 5a**
POM reaction scheme over supported Pt adapted from the proposition of de Smet et al. to account for reversible oxygen adsorption, carbon species oxidation and $CO_2$ formation.

| Reaction | A or $s^0$ ($Pa^{-1}$ $s^{-1}$ or $s^{-1}$) | $E_{act}$ (kJ $mol^{-1}$) | Rate equation | Step |
|---|---|---|---|---|
| $O_{2,g} + 2^* \rightarrow 2O^*$ | 0.11 | 0 | $k_{1a}P_{O_2}\theta_*$ | 1a |
| $2O^* \rightarrow O_{2,g} + 2^*$ | $1.7 \times 10^{13}$ | 200 | $k_{1b}\theta^2_O$ | 1b |
| $CH_{4,g} + 2O^* \rightarrow C^* + 2H_2O_g + ^*$ | $2.4 \times 10^5$ | 48.2 | $k_2P_{CH_4}\theta^2_O$ | 2 |
| $C^* + O^* \rightarrow CO^* + ^*$ | $1 \times 10^{13}$ | 62.8 | $k_{3a}\theta_C\theta_O$ | 3a |
| $CO^* + ^* \rightarrow C^* + O^*$ | $1 \times 10^{11}$ | 184 | $k_{3b}\theta_{CO}\theta_*$ | 3b |
| $CO^* + O^* \rightarrow CO_{2,g} + 2^*$ | $1.9 \times 10^9$ | 30 | $k_{4a}\theta_{CO}\theta_O$ | 4a |
| $CO_{2,g} + 2^* \rightarrow CO^* + O^*$ | $6.3 \times 10^2$ | 28 | $k_{4b}P_{CO_2}\theta^2_*$ | 4b |
| $CO^* \rightarrow CO_{v,g} + ^*$ | $1 \times 10^{13}$ | 126 | $k_{5a}\theta_{CO}$ | 5a |
| $CO_{v,g} + ^* \rightarrow CO^*$ | 0.84 | 0 | $k_{5b}P_{CO}\theta_*$ | 5b |

* denotes a Pt active site or a site located on the ceria, see Section 5, $k_x$ denotes the term $A_x \exp(-E_{act,x}/RT)$ or $s^0{}_x \exp(-E_{act,x}/RT)$, respectively.

activation energy for the methane activation step were estimated by a regression analysis of the experimental CO selectivities. All the other kinetic parameters of the remaining 4 steps were fixed at values obtained from the literature. The above reaction model gave an adequate description of their experimental data [17].

In the present work, the above model could describe most of the data in this study adequately (estimated kinetic parameters are indicated in Table 4), except the data concerning the $CO_2$ addition. Remarkably, it should be mentioned that de Smet et al. [17] never performed $CO_2$ addition experiments. Despite the reasonable fit for methane and oxygen conversion as well as for the carbon oxide selectivity in cases without $CO_2$ addition, there is a need to extend the suggested five-step reaction model (Table 4).

The latter model identified as partially suitable was kept as starting point for a kinetic description of data in the present work. However, for fitting all the data in this study, several steps had to be formulated reversibly. In order to take into account the addition of $CO_2$ in the reactant feed, step 4 has been assumed reversible. In order to account for a reversibility of the initial carbon species oxidation the step 3 was also considered as reversible. Furthermore, Temporal-Analysis-of-Products (TAP) experiments [18] have shown that oxygen adsorption on platinum is reversible at the reaction temperatures investigated and a Temperature-Programmed-Desorption (TPD) study not presented in this work supported this for the case of the investigated catalyst under the applied reaction conditions. The extended reaction network used in this work is reported in Table 5a and the involved steps are the following:

*Oxygen adsorption*. The first step in the reaction mechanism concerns the activation of oxygen through dissociative adsorption. According to Williams et al. [19], the adsorption rate can be assumed to be first order in the fraction of vacant surface sites $\theta^*$, which implies that the rate-determining step in the adsorption involves the interaction of molecular oxygen with a single catalytic site. It is worth to note that the rate equations for our models considering an oxygen assisted methane activation (step 1 in Table 4 and also step 1a in the extended model given in Table 5a) account for a first order in vacant sites, while the balance obviously imposes that an adsorption of one oxygen molecule will occupy two free sites. Oxygen adsorption is considered to be competitive, in contrast to the mechanism proposed by Hickman and Schmidt [20].

*Methane adsorption*. In agreement with theoretical calculations of Au et al. [21], methane adsorption under the present conditions is considered to be oxygen-assisted, directly resulting in adsorbed hydroxyl species that recombine instantaneously to gaseous water. Thus a dissociative adsorption of methane, resulting in the formation of a surface carbon species and gaseous water, is taken into account in step 2.

Reaction 2 is obviously not an elementary step, but proceeds through a number of intermediates such as adsorbed $CH_x$ ($x = 1,3$) fragments and adsorbed OH species. Molecular methane adsorption on the Pt surface is considered to be reversible and in quasi equilibrium. The abstraction of the first hydrogen atom by adsorbed oxygen species is considered as the rate-determining step in methane decomposition. The subsequent abstraction of hydrogen atoms from adsorbed $CH_x$ fragments, and the recombination of hydroxyl species to water, is potentially very fast. As a result, no $CH_x$ species appear as surface intermediates in the kinetic model.

*Carbon monoxide and carbon dioxide production*. Steps 3–5 concern paths toward carbon monoxide and carbon dioxide. Reaction 3 describes the formation of adsorbed CO species, which is generally considered to be very fast [20]. Adsorbed CO species are converted to $CO_2$ in step 4, which desorbs instantaneously. $CO_2$ adsorption is not taken into account in the kinetic model, since the heat of adsorption of $CO_2$ on Pt is very low [22]. Finally, CO desorption and adsorption are described in the kinetic model by steps 5a and 5b.

As mentioned before and detailed in a later paragraph, the reaction scheme adapted from de Smet et al. in Table 5a allows a reasonable description of the methane conversion and carbon oxide selectivities observed. On the other hand, the hydrogen production is not described and the experimental results indicated a selectivity of up to 25%. In order to account for the hydrogen production, the following step was added for adapting the mechanism by de Smet et al. presented in Table 5a:

$H_2O + * \rightarrow H_2 + O*$ (equation of step 6 adding to Table 5a, rate expression : $k_6P_{H_2O}\theta_*$)

Using estimated values for the pre-exponential factor of $6.6 \times 10^{12}$ $s^{-1}$ and an activation energy of 173 kJ/mol and a slightly lower sticking coefficient for oxygen adsorption, the hydrogen selectivity is adequately described as shown in Fig. 3.

However, an alternative reaction mechanism using elements of the work from Hickman and Schmidt [20] was established. In this case $H_2$ is produced by the recombination of adsorbed atomic hydrogen formed directly by an abstraction from methane or water on reduced platinum sites and is summarized in Table 5b.

The reversible steps 1, 3, 4, 5 are identical to those included in the adapted scheme following de Smet et al. presented in Table 5a. The essential difference in this scheme from Table 5b over that previous presented in Table 5a is found in step 2 now considering a dissociation of methane into a carbon species and adsorbed hydrogen as proposed by Hickman and Schmidt [20]. Consequently, step 6 accounts for reversible hydrogen release and step 7 accounts for its reversible oxidation to gaseous water. In fact, without anticipating

**Table 5b**
POM reaction scheme over supported Pt proposed in this study accounting for hydrogen production.

| Reaction | A or $s^0$ ($Pa^{-1}$ $s^{-1}$ or $s^{-1}$) | $E_{act}$ (kJ $mol^{-1}$) | Rate equation | Step |
|---|---|---|---|---|
| $O_{2,g} + 2^* \rightarrow 2O^*$ | 0.68 | 0 | $k_{1a}P_{O_2}\theta^2_*$ | 1a |
| $2O^* \rightarrow O_{2,g} + 2^*$ | $1.0 \times 10^{14}$ | 200 | $k_{1b}\theta^2_O$ | 1b |
| $CH_{4,g} + 5^* \rightarrow C^* + 4H^*$ | $9.35 \times 10^3$ | 125.2 | $k_2P_{CH_4}\theta^5_*$ | 2 |
| $C^* + O^* \rightarrow CO^* + ^*$ | $1 \times 10^{13}$ | 62.8 | $k_{3a}\theta_C\theta_O$ | 3a |
| $CO^* + ^* \rightarrow C^* + O^*$ | $1 \times 10^{11}$ | 184 | $k_{3b}\theta_{CO}\theta_*$ | 3b |
| $CO^* + O^* \rightarrow CO_{2,g} + 2^*$ | $3.2 \times 10^{13}$ | 37.4 | $k_{4a}\theta_{CO}\theta_O$ | 4a |
| $CO_{2,g} + 2^* \rightarrow CO^* + O^*$ | $9.9 \times 10^3$ | 10 | $k_{4b}P_{CO_2}\theta^2_*$ | 4b |
| $CO^* \rightarrow CO_{v,g} + ^*$ | $1 \times 10^{13}$ | 126 | $k_{5a}\theta_{CO}$ | 5a |
| $CO_{v,g} + ^* \rightarrow CO^*$ | 0.71 | 0 | $k_{5b}P_{CO}\theta_*$ | 5b |
| $2H^* \rightarrow H_{2,g} + 2^*$ | $1.0 \times 10^{14}$ | 159.7 | $k_{6a}\theta^2_H$ | 6a |
| $H_{2,g} + 2^* \rightarrow 2H^*$ | 0.02 | 0 | $k_{6b}P_{H_2}\theta^2_*$ | 6b |
| $2H^* + O^* \rightarrow H_2O_{v,g} + 3^*$ | $1.0 \times 10^{13}$ | 20 | $k_{7a}\theta^2_H\theta_O$ | 7a |
| $H_2O_{v,g} + 3^* \rightarrow 2H^* + O^*$ | $1.0 \times 10^6$ | 69 | $k_{7b}P_{H_2O}\theta^3_*$ | 7b |

* denotes a Pt active site or a site located on the ceria, see Section 5, $k_x$ denotes the term $A_x \exp(-E_{act,x}/RT)$ or $s^0{}_x \exp(-E_{act,x}/RT)$, respectively.

**Table 6a**
Matrix indicating the required linear combination relating the reaction rates to the change in species concentration or coverage for the kinetic model presented in Table 5a.

| | 1a | 1b | 2 | 3a | 3b | 4a | 4b | 5a | 5b |
|---|---|---|---|---|---|---|---|---|---|
| $O_{2,g}$ | −1 | 1 | | | | | | | |
| O* | 2 | −2 | −2 | −1 | 1 | −1 | 1 | | |
| $CH_{4,g}$ | | | −1 | | | | | | |
| C* | | | 1 | −1 | 1 | | | | |
| CO* | | | | 1 | −1 | −1 | 1 | −1 | 1 |
| $CO_{2,g}$ | | | | | | 1 | −1 | | |
| $CO_g$ | | | | | | | | 1 | −1 |
| $H_2O_{,g}$ | | | 2 | | | | | | |

the discussion, the rapid release of hydrogen observed during TAP experiments supports formulating step 2 in the present form, while the increasing catalyst activity adding more oxygen pre-pulses is more contradicting a methane activation without participation of oxygen.

Parameter fitting according to the newly proposed reaction scheme in Table 5a was restricted to a minimum using literature data and other criteria to estimate parameters. Hickman and Schmidt [20] give rate parameters for the reverse reaction of step 3, which has been included in our mechanism (3b). Only the parameters of steps 1a, 4a and 4b have been optimized through regression analysis of 70 data points. Note that only 5 parameters have been adjusted.

The (partial) description of results by the model adapted from de Smet et al. (considered steps and estimated kinetic parameters as given in Table 5a) is depicted showing the experimentally observed performances (points) along with the model predicted ones (lines) in Fig. 4a and by the respective parity plots for the methane conversion and carbon monoxide selectivity in Fig. 5a. Resulting from the fact that this model does not account for a hydrogen release the oxygen consumption is over-estimated and the calculated resulting oxygen conversions do not correspond to the measured oxygen conversion. Hence, the Fig. 4a below shows only the experimental oxygen conversion and the hydrogen selectivity was not included in Fig. 5a. An adequate description of both the methane conversion and the CO selectivity are obtained.

Extending the reaction scheme adapted form de Smet et al. [17] to the mechanism given in Table 5b allowed to account for a hydrogen production. However, as only one step was replaced (step 2) and two more were added (steps 6 and 7) several parameters could remain fixed to values determined for the above discussed scheme outlined in Table 5a. This relates to the steps 3a, 3b and 5a. Other parameters needed only an adjustment of the frequency factor, which was the case for steps 1a, 1b, 5b. This relates to the fact that changing step 2 from an "oxygen assisted" one to a step without oxygen participation required obviously to adapt to the different needs in oxygen consumption. The parameters of the "new" steps 2, 6 and 7 were obviously newly estimated, but also the parameters of the step 4 relating to CO oxidation had been estimated once more.

**Table 6b**
Matrix indicating the required linear combination relating the reaction rates to the change in species concentration or coverage for the kinetic model presented in Table 5b.

| | 1a | 1b | 2 | 3a | 3b | 4a | 4b | 5a | 5b | 6a | 6b | 7a | 7b |
|---|---|---|---|---|---|---|---|---|---|---|---|---|---|
| $O_{2,g}$ | −1 | 1 | | | | | | | | | | | |
| O* | 2 | −2 | | −1 | 1 | −1 | 1 | | | | | −1 | 1 |
| $CH_{4,g}$ | | | −1 | | | | | | | | | | |
| C* | | | 1 | −1 | 1 | | | | | | | | |
| CO* | | | | 1 | −1 | −1 | 1 | −1 | 1 | | | | |
| $CO_{2,g}$ | | | | | | 1 | −1 | | | | | | |
| H* | | | 4 | | | | | | | −2 | 2 | −2 | 2 |
| $H_{2,g}$ | | | | | | | | | | 1 | −1 | | |
| $H_2O_{,g}$ | | | | | | | | | | | | 1 | −1 |
| $CO_g$ | | | | | | | | 1 | −1 | | | | |

All fitted kinetic parameters are given in Table 5b along with a comparison of the experimentally observed performances (points) and the model predicted ones (lines) in Fig. 4b and the respective parity plots for the methane conversion and carbon monoxide and hydrogen selectivity in Fig. 5b as a measure of the fitting quality.

The main result of using the new reaction scheme is a reasonable description of the hydrogen production and a better description of the oxygen conversion depicted in Fig. 4b. Nevertheless, especially at high residence times (W/F) there is a major deviation in the model predicted oxygen conversion against the experimental one. Initially only one type of active site is assumed, although this will be discussed in more details in the next section.

## 5. Discussion

The above section on kinetic modeling indicated that a reasonable description was achieved. Nevertheless, the proposed models in Tables 5a and 5b have some fundamental differences requiring an appropriate discussion in the following.

### 5.1. Evaluation of the different proposed models

As can be seen in Figs. 4a and 5a the modified "oxygen assisted" CPOM mechanism originally proposed by de Smet et al. [17] describes adequately the $CH_4$ conversion and CO selectivity data over the Pt/PrCeZrO/α-$Al_2O_3$ monolith catalyst, although some of the values of the kinetic parameters are significantly different. This will be explained below by taking the role of the support into consideration. The extension (Table 5a) to the original scheme (Table 4) was found necessary to describe experiments with $CO_2$ addition not performed in the de Smet et al. work. As was noted before, de Smet et al. studied the reaction in a continuous flow reactor set-up with a single wire Pt gauze as catalyst [9,17]. It seems logical that readsorption could be underrepresented under these conditions and that might have prevented the authors to discriminate the steps newly added in this work. In fact these steps were apparently not needed to describe the smaller base of experimental data with their proposed reaction network. However, the new experiments with carbon dioxide addition to the feed indicated that several steps in the carbon oxide formation proceed in fact reversibly.

The global rate coefficient for dissociative adsorption of methane is the product of the equilibrium coefficient for molecular adsorption and the rate coefficient of the rate-determining step. The activation energy of the rate-determining step thus can be written as

$$E_{act} = E^{global} - \Delta H^0_{ads} \quad (8)$$

where $E^{global}$ is the global activation energy of dissociative methane adsorption, and $\Delta H^0$ is the standard adsorption enthalpy of methane. Substitution of the estimated global activation energy, 48.2 kJ mol$^{-1}$, and the standard adsorption enthalpy of methane, $\Delta H$ = −25.1 kJ/mol [22], results in an activation energy of the rate-determining step of 73.3 kJ mol$^{-1}$.

In the literature, no data were found regarding the activation energy of oxygen-assisted methane adsorption. The calculated value, however, is higher than the reported activation energy of 43.1 kJ mol$^{-1}$ [23] for dissociative methane adsorption into adsorbed carbon and hydrogen species.

The second further extended model (Table 5b) allowed both a satisfying prediction of the $H_2$ selectivity and a reasonable prediction of the $O_2$ conversion. New parameter estimation could be

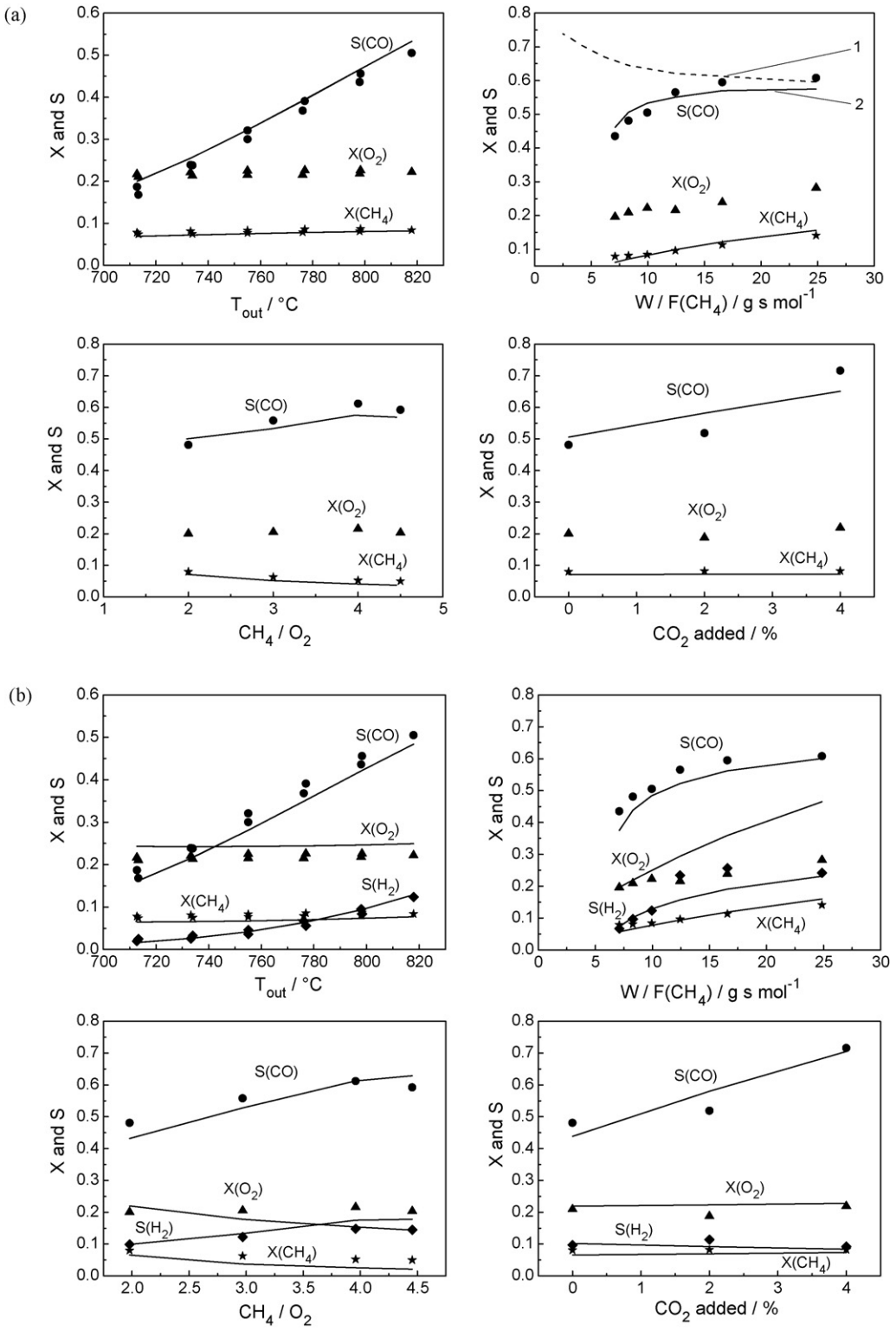


**Fig. 4.** (a) Experimental and calculated data at different process parameters using the mechanism adapted from de Smet et al. Trace 1 denotes the CO selectivity if the temperature would remain constant and trace 2 outlines the CO selectivity at the experimentally measured temperatures altered by the convective contribution. (b) Experimental and calculated data at different process parameters using the mechanism proposed in this work.

limited to newly introduced reaction steps and a reevaluation of the parameters for the reversible CO oxidation in step 4.

On the other hand the major change for this model is the assumption of a "not oxygen assisted" activation of methane as proposed by Hickman and Schmidt [20]. Assuming an activation of methane via the formation of a carbon species and adsorbed hydrogen rapidly releasable to gas-phase agrees well with the observed pulse shaped rapid formation of $H_2$ in TAP experiments over this catalyst [24]. In turn, this is somewhat contradictory to the rising catalyst activity with increasing amount of pre-adsorbed oxygen reported in the same work. Moreover, the least satisfying description of the model is observed for the oxygen conversion at long

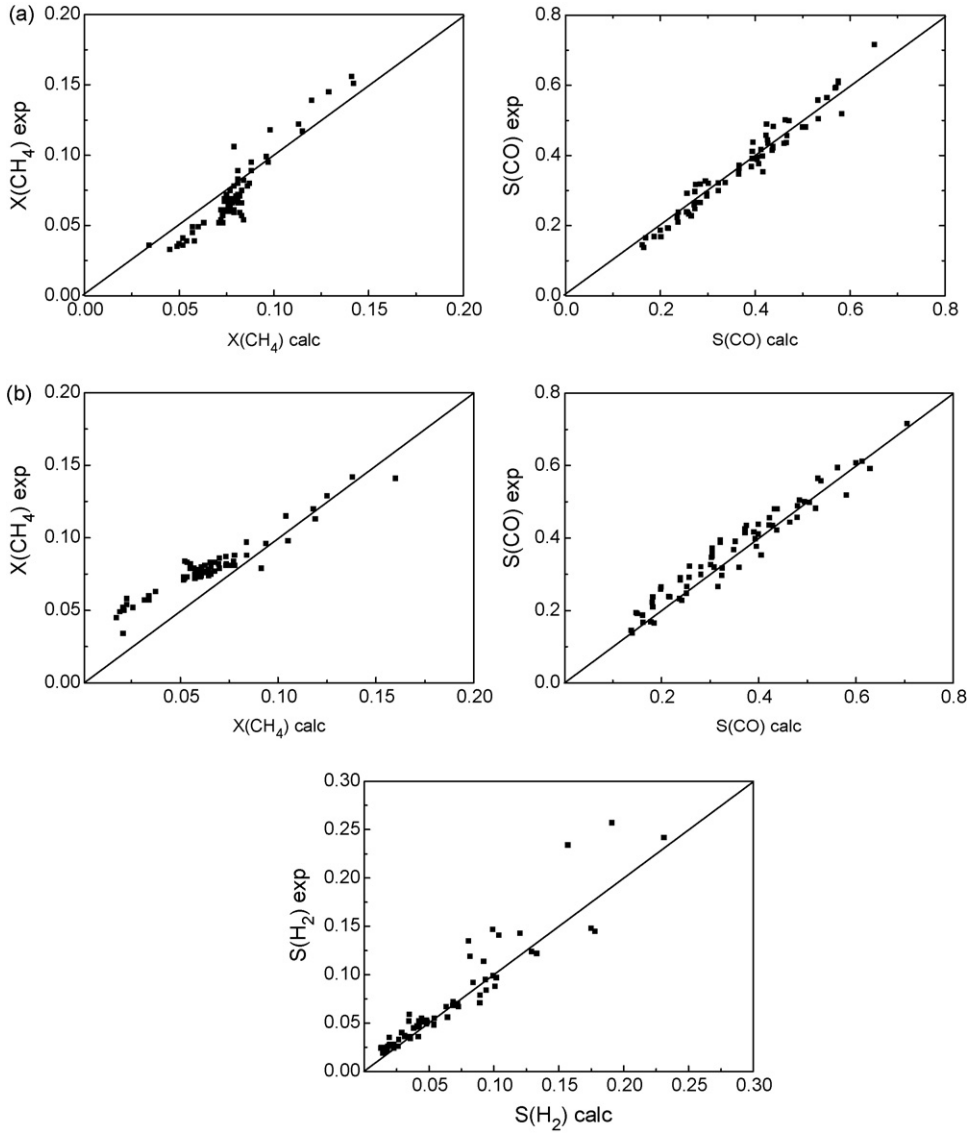


**Fig. 5.** (a) Parity plot for the methane conversion and the CO selectivity of experimental and calculated values (according to the kinetic parameters given in Table 5a). (b) Parity plot for the methane conversion, the CO and $H_2$ selectivity of experimental and calculated values (according to the kinetic parameters given in Table 5b).

contact times (high W/F) without observing a strong detrimental impact on the prediction of other reaction observables. Both deviations could be rationalized to some extend assuming that oxygen is also activated or stored on another less reactive site, at a lower rate than that for the now assumed single site. Under TAP conditions this second type site would become active only at more pronounced oxygen pre-adsorption and at ambient pressure its impact would increase with rising contact time. In fact assuming such a second type site is even reasonable given the previously demonstrated participation of oxygen on the support or even in its bulk, leading to a small catalytic activity of the support material under atmospheric pressure. Despite being out of the scope of the present kinetic investigation focusing on description of the dominating reactions (most probably proceeding on Pt sites) the above suggests a deeper discussion on the role of ceria in the mechanistic scheme.

### 5.2. Role of ceria

Whereas the assumption of a single active site for methane and oxygen activation seems quite relevant over pure Pt catalysts (gauzes), although in their original reaction mechanism Hickman and Schmidt [20] proposed different sites for methane and oxygen, it is certainly not the case for a Pt/PrCeZrO/α-$Al_2O_3$ monolith catalyst. The ceria can activate CO and water as well and adsorb different reaction intermediates such as hydroxyl groups and carbonates. This will lead to parallel reactions pathways for the oxidation of methane over these catalysts. This has been demonstrated in the case of three-way catalysts [25].

Steady-state kinetics will not be able in most cases to unequivocally discriminate between these different pathways due to the strong coupling of the kinetic constants in these similar paths. However, by comparing results, including the values of the kinetic parameters, of experiments over platinum and Pt/PrCeZrO/α-$Al_2O_3$ monolith catalysts the role of the support can be unraveled. Therefore in this work we compare our results over Pt/PrCeZrO/α-$Al_2O_3$ single channel of monolith to the results of de Smet et al. over a Pt gauze [17]. Both sets of data have been obtained under rather similar conditions under mass transfer limitations, although over different catalyst geometries. Moreover both data sets have been analyzed and modeled through a similar sequence of elementary steps.

From Fig. 4a it is observed that the CO selectivity increases from 20 to 50% over a temperature interval of 100 °C. In the case of the Pt

gauze this increase is lower from 20 to 35% only. The CO selectivity depends on the ratio of the CO desorption rate and the CO oxidation rate to $CO_2$, i.e. R5 and R4. The temperature dependence of the CO selectivity depends thus on the ratio of the activation energies of these two rates. Thus, for E5/E4 and with E5 fixed at 126 kJ/mol this becomes E4 (Pt/PrCeZrO/α-$Al_2O_3$) < E4 (Pt gauze). This is indeed the case shown in Tables 4 and 5. Thus the ceria effectively lowers the activation barrier of the $CO_2$ production rate. Indeed Nibbelke et al. [25] found from transient experiments of CO oxidation over a Pt/Rh/Ce/Al catalyst that a parallel $CO_2$ route involving species adsorbed on ceria exists. They proposed the following reaction step:

$$CO* + Os \rightarrow CO_{2,g} + * + s$$

where * represents a Pt site and s a ceria site. They have estimated an activation energy for this step of 11 kJ/mol. The value obtained in our study of 30 kJ/mol is in between the values of the pathway over Pt and the ceria-catalyzed route, thus indicating that both routes play a role for $CO_2$ production over the Pt/Ce/Al catalyst.

Fig. 4a and b shows an increasing CO selectivity with increasing space-time quite contrary to the effect observed over the Pt gauze. In fact with increasing flow rates more heat is removed from the reactor and the catalyst temperature is lower at constant settings of the reactor furnace. The temperatures measured with the thermocouple on the monolith wall thus decrease with increasing flow rates. The effect of the change in temperature on the CO conversion is larger than the effect of contact time. Therefore the dotted line 1 in Fig. 4a is a simulation with a constant catalyst temperature of 850 °C. Now the CO selectivity decreases with increasing space-time indicating that CO is the most important primary product in the partial oxidation of methane. These results are well in line with TAP studies [20] as well as steady state experiments [26].

Similar methane conversions are obtained for the Pt/PrCeZrO/α-$Al_2O_3$ catalyst and the Pt gauze at apparently very different W/F values (5–25 vs. 10–130 g s $mol^{-1}$). The number of surface Pt atoms of the gauze has been estimated to be 4–6 nmol using data from [27] corrected for the different gauze diameters. The monolith contains approximately 30 nmol of surface platinum atoms ($D \sim 50\%$). The actual space-times with respect to the number of surface platinum atoms in both reactors are thus very similar.

Fig. 4a and b shows that addition of $CO_2$ to the feed lead to a higher CO selectivity. Unfortunately, these experiments have not been reported by de Smet et al. [17] over the Pt gauze. In our case the $CO_2$ co-feeding experiments can be accounted for in the model by assuming a dissociation of $CO_2$ into adsorbed CO and O. Carbon dioxide dissociation over platinum is debated in the literature. Tol et al. [28] reported that $CO_2$ does not dissociate over Pt but Huinink [29] has observed oxygen exchange of $CO_2$. TAP experiments over Pt/$Al_2O_3$ using labeled $CO_2$ showed that there is no occurring of $CO_2$ dissociation or a direct reaction between $CO_2$ and adsorbed carbon neither [30]. However, similar TAP experiments over Pt/$ZrO_2$ showed that $CO_2$ dissociations occurs where the oxygen vacancy on the $ZrO_2$ catalyzes this step [30]. In this case $CO_2$ dissociation involves sites on the ceria.

The value of the oxygen sticking coefficient of 0.11 over Pt/PrCeZrO/α-$Al_2O_3$ is almost an order of magnitude higher than over Pt reported in the range of 0.01 [17]. This is in agreement with an activation of oxygen on the ceria.

### 5.3. Rate-determining step

Using Campbell's definition for the degree of rate control [31]:

$$X_{rc,i} = \left(\frac{k_i}{r}\right)\left(\frac{\delta r}{\delta k_i}\right) \quad (9)$$

**Table 7a**
Degree of rate control ($X_{rc,i}$) for the 5 reversible reaction steps from Table 5a for the $CH_4$, $O_2$, CO and $CO_2$ gas phase species.

| Step | $CH_4$ | $O_2$ | CO | $CO_2$ |
|---|---|---|---|---|
| 1 | 0.06 | 0.00 | 0.47 | −0.45 |
| 2 | 0.51 | 0.55 | −0.28 | 0.27 |
| 3 | 0.01 | 0.00 | 0.09 | −0.08 |
| 4 | −0.04 | 0.02 | −0.43 | 0.41 |
| 5 | 0.00 | 0.00 | 0.00 | 0.00 |

the rate-controlling steps can be established. In (Eq. (9)) where $X_{rc,i}$ is the degree of rate control and $r$ is the overall rate, the partial derivative is taken holding constant the equilibrium constant for step $i$ and the rate constants $k_j$ for all other steps $j$. Table 7a gives the $X_{rc,i}$ as defined by (Eq. (9)) above for the 5 reversible reaction steps from Table 5a for the 4 principal gas phase species. These coefficients can vary between −1 and +1. A high absolute value indicates that the step has a large contribution to the overall reaction rate [31]. Note that step (1) has been taken reversible by introducing a small rate constant for the reverse step. Within a certain range of values this did not influence the modeling results.

From Table 7a it follows that the production of CO in the reaction scheme proposed in Table 5a depends mainly on three steps. Higher CO production rates can be obtained by either increasing the methane activation step (1), or lower the oxygen activation step (2) or lower the adsorbed CO oxidation rate (4). On the other hand changing the CO desorption rate (5) does not influence the CO production rate.

Table 7b shows the data for performing a similar analysis for the case to the reaction scheme presented in Table 5b. In fact, it is clear that the adsorption of oxygen (step 1) followed by the oxidation of the carbon species (step 3) has a high impact on the formation of the selective products like CO and $H_2$. In the case of CO these two steps dominate even over the oxidation of adsorbed CO and its release to the gas phase oxygen has a still smaller impact.

There is a substantial difference for the hydrogen formation as the sorption has the strongest impact here and the oxidation of hydrogen has approximately the same importance as the oxygen adsorption. Nevertheless, considering the importance of the oxygen adsorption, thus the local oxygen coverage, and the above discussed role of ceria sites, it becomes clear why an oxygen exchange between Pt and ceria sites, i.e. the oxygen storage capacity of the support has such a prominent importance for the catalyst performance.

The microkinetic model offers thus an aid in catalyst development. On the other hand developing kinetic models based on rate-equation containing a single RDS will not capture all the details of the partial oxidation of methane mechanism.

### 5.4. Influence of mass transfer phenomena

Similar to the findings of de Smet et al. [17] we obtained higher methane and oxygen conversions and better CO selectivity in simulations in the absence of diffusion limitations.

**Table 7b**
Degree of rate control ($X_{rc,i}$) for the 7 reversible reaction steps from Table 5b for the $CH_4$, $O_2$, CO, $CO_2$, $H_2$ and $H_2O$ gas phase species.

| Step | $CH_4$ | $O_2$ | CO | $CO_2$ | $H_2$ | $H_2O$ |
|---|---|---|---|---|---|---|
| 1 | 0.85 | 0.97 | −0.51 | 0.40 | −0.78 | 0.09 |
| 2 | −0.41 | −0.47 | 0.29 | −0.23 | 0.44 | −0.05 |
| 3 | 0.15 | 0.06 | 0.42 | −0.33 | 0.68 | −0.08 |
| 4 | −0.08 | −0.03 | −0.41 | 0.32 | 0.08 | −0.01 |
| 5 | 0.06 | 0.02 | 0.34 | −0.27 | −0.06 | 0.01 |
| 6 | 0.07 | 0.03 | −0.04 | 0.03 | 0.83 | −0.09 |
| 7 | −0.06 | −0.02 | 0.06 | −0.05 | −0.74 | 0.08 |

## 6. Conclusions

In the present paper the kinetics of the partial oxidation of methane has been studied over a Pt/PrCeZrO/α-$Al_2O_3$ supported on a triangular monolith. By running high flow velocities and using a suitable preheating, nearly isothermal conditions were obtained inside the monolith channel. Furthermore the catalyst temperature was measured directly by placing a thermocouple at the outside of a single monolith channel. This mode of catalyst testing together with a relatively simple reactor model, a one-dimensional model that takes the mass transfer limitations into account, allowed accessing the intrinsic reaction conditions.

A kinetic model based on 5 elementary steps for the oxidation of methane over platinum has shown already a reasonable description of the $CH_4$ conversion and CO selectivity. Including a sixth step where water (re)adsorbs and decomposes into gas-phase hydrogen and adsorbed oxygen allows even obtaining a mechanism with oxygen-assisted methane activation capable to describe additionally the experimentally observed hydrogen formation. Nevertheless, it should be pointed out that the sixth step can be regarded as "formal" reaction, specifically as it could be the observed net result combining a rapidly occurring water-gas shift reaction [32] with the $CO_2$ (re)adsorption step 4b listed in Table 5a.

Another extended kinetic model based on 7 elementary steps considers that oxygen does not assist in the methane activation. This model summarized in Table 5b has been validated and it allowed at short contact time a satisfying description of the experimental data. Nevertheless, at longer contact times, slower steps not considered in the present scheme gain apparently in relative importance. On the other hand, much more experimental data beyond the scope to this work would be needed to ensure proper parameter estimation for these extra steps. The same applies to reinforcing the estimation of parameters for the hydrogen production requiring, e.g. an addition of hydrogen to the reactant mixture.

The data over the Pt/PrCeZrO/α-$Al_2O_3$ catalyst have been compared to literature data over a Pt gauze. In this way the role of ceria can be unraveled. Ceria provides a parallel reaction pathway for the oxidation of CO with a much lower energy barrier than over Pt. The kinetic model takes into account the co-feeding of carbon dioxide thus the methane dry reforming. This occurs through the dissociation of carbon dioxide catalyzed by ceria. A reaction path analysis has revealed the main reaction steps for the production of carbon monoxide.

Given that both kinetic models yield within their limits a reasonable description of the experimental data, but that they differ strongly in their assumptions concerning the methane activation step, i.e. oxygen assisted variant for the scheme presented in Table 5a and not oxygen assisted variant for the scheme presented in Table 5b, it seems that it currently not possible to identify a more probable alternative. Despite the fact that a recent TAP study [24] indicated a facile and rapid formation of hydrogen during the activation of methane, it cannot be excluded that oxygen still participates in this process reacting only with a part of the hydrogen abstracted from the methane. Nevertheless, being not able to express a clear favor for an oxygen assisted or not oxygen assisted variant of the kinetic model tentatively suggests that the activation of methane is not the most rate limiting step in the reaction network proceeding on the catalyst. This however, is in good agreement the observation of a fast formation of hydrogen as sharp pulse response in the formerly mentioned TAP study.

## Acknowledgements

This work was performed and supported in framework of the joined European laboratory (LEA-313) between France and Russia on catalysis (LFRC). Financial support by the RFBR-CNRS 05-03-34761 project and support of the PhD thesis of E.L. Gubanova by the France Embassy Grant are gratefully acknowledged.

## References

[1] S. Cornot-Gandolphe, Changes in world gas reserves and resources, J. Energy Explore. Exploit. 13 (1995) 3–17.
[2] British Petroleum, Review of World Gas, B.P. Gas International, London, 1987.
[3] P.D.F. Vernon, M.L.H. Green, A.K. Cheetham, A.T. Ashcroft, Partial oxidation of methane to synthesis gas, and carbon dioxide as an oxidising agent for methane conversion, Catal. Today 13 (1992) 417–426.
[4] D.A. Hickman, L.D. Schmidt, Production of syngas by direct catalytic oxidation of methane, Science 259 (1993) 343–346.
[5] A.B. Mhadeshwar, D.G. Vlachos, A catalytic reaction mechanism for methane partial oxidation at short contact times, reforming, and combustion, and for oxygenate decomposition and oxidation on platinum, Ind. Eng. Chem. Res. 46 (2007) 5310–5324.
[6] V.A. Sadykov, T.G. Kuznetsova, Yu.V. Frolova-Borchert, G.M. Alikina, A.I. Lukashevich, V.A. Rogov, V.S. Muzykantov, L.G. Pinaeva, E.M. Sadovskaya, Yu.A. Ivanova, E.A. Paukshtis, N.V. Mezentseva, L.Ch. Batuev, V.N. Parmon, S. Neophytides, E. Kemnitz, K. Scheurell, C. Mirodatos, A.C. van Veen, Fuel-rich methane combustion: role of the Pt dispersion and oxygen mobility in a fluorite-like complex oxide support, Catal. Today 117 (2006) 475–483.
[7] E.L. Gubanova, A. van Veen, C. Mirodatos, V.A. Sadykov, N.N. Sazonova, Influence of the mobility of oxygen in a complex oxide carrier on the mechanism of partial oxidation of methane, Russ. J. Gen. Chem. 78 (2008) 2191–2202.
[8] A. Beretta, P. Baiardi, D. Prina, P. Forzatti, Analysis of a catalytic annular reactor for very short contact times, Chem. Eng. Sci. 54 (1999) 765–773.
[9] C.R.H. de Smet, M.H.J.M. de Croon, R.J. Berger, G.B. Marin, J.C. Schouten, An experimental reactor to study the intrinsic kinetics of the catalytic partial oxidation of methane in the presence of heat-transport limitations, Appl. Catal. A: Gen. 187 (1999) 33–48.
[10] G.F. Froment, K.B. Bischoff, Chemical Reactor Analysis and Design, 2nd ed., Wiley, 1990, 704 p.
[11] S.T. Sie, Miniaturization of hydroprocessing catalyst testing systems: theory and practice, AIChE J. 42 (2004) 3498–3507.
[12] G. Groppi, A. Belloni, E. Troncani, P. Forzatti, A comparison of lumped and distributed models of monolith catalytic combustors, Chem. Eng. Sci. 50 (1995) 2705–2715.
[13] R.E. Hayes, S.T. Kolaczkowski, Introduction to Catalytic Combustion, Gordon and Breach Science Publishers, 1997, 681 p.
[14] H.W. Brauer, F. Fetting, Stofftransport bei Wandreaktion im Einlaufgebiet eines Strömungsrohres, Chem. Ing. Technol. 38 (1966) 30–35.
[15] R.C. Reid, J.M. Prausnitz, B.E. Poling, The Properties of Gases and Liquids, 4th ed., McGraw Hill, New York, 1998.
[16] A.C. Hindemarsh, ODEPACK, A Systematized Collection of ODE Solvers, Elsevier, 1983, pp. 55–64.
[17] C.R.H. de Smet, M.H.J.M. de Croon, R.J. Berger, G.B. Marin, J.C. Schouten, Kinetics for the partial oxidation of methane on a Pt gauze at low conversions, AIChE J. 46 (2000) 1837–1849.
[18] M. Fathi, F. Monnet, Y. Schuurman, A. Holmen, C. Mirodatos, Reactive oxygen species on platinum gauzes during partial oxidation of methane into synthesis gas, J. Catal. 190 (2000) 439–445.
[19] W.R. Williams, C.M. Marks, L.D. Schmidt, Steps in the reaction $H_2 + O_2 \leftrightarrow H_2O$ on Pt:OH desorption at high temperatures, J. Phys. Chem. 96 (1992) 5922–5931.
[20] D.A. Hickman, L.D. Schmidt, Step in $CH_4$ oxidation on the Pt and Rh surface: high-temperature reactor simulations, AIChE J. 39 (1993) 1164–1177.
[21] C.-T. Au, C.-F. Ng, M.-S. Liao, Methane dissociation and syngas formation on Ru, Os, Rh, Ir, Pd, Pt, Cu, Ag and Au: a theoretical study, J. Catal. 185 (1999) 12–22.
[22] E. Shustorovich, The bond-order conservation approach to chemisorption and heterogeneous catalysis: applications and implications, Adv. Catal. 37 (1990) 101–164.
[23] A.B. Anderson, J.J. Moloney, Activation of methane on iron, nickel, and platinum surfaces. A molecular orbital study, J. Phys. Chem. 92 (1988) 809–812.
[24] E.L. Gubanova, A. van Veen, C. Mirodatos, V.A. Sadykov, N.N. Sazonova, Influence of the oxygen mobility in complex oxide supports on the mechanism of the partial oxidation of methane, Russ. Chem. J. 52 (2008) 21–31.
[25] R.H. Nibbelke, A.J.L. Nievergeld, J.H.B.J. Hoebink, G.B. Marin, Development of a transient kinetic model for the CO oxidation by $O_2$ over a Pt/Rh/$CeO_2$/γ-$Al_2O_3$ three-way catalyst, Appl. Catal. B: Environ. 19 (1998) 245–259.
[26] F. Monnet, Y. Schuurman, F. Cadete Santos Aires, J.C. Bertolini, C. Mirodatos, Silicon nitride supported platinum catalysts for the partial oxidation of methane at high temperatures, Catal. Today 64 (2001) 51–58.
[27] E. Bergene, O. Tronstad, A. Holmen, Surface areas of Pt–Rh catalyst gauzes used for ammonia oxidation, J. Catal. 146 (1994) 141–147.
[28] M.F.H. van Tol, A. Gielbert, B.E. Nieuwenhuys, The adsorption and dissociation of $CO_2$ on Rh, Appl. Surf. Sci. 67 (1993) 166–178.
[29] J.P. Huinink, Doctorate Thesis, Eindhoven University of Technology, The Netherlands, 1995.

[30] A.M. O'Connor, Y. Schuurman, J.R.H. Ross, C. Mirodatos, Transient studies of carbon dioxide reforming of methane over $Pt/ZrO_2$ and $Pt/Al_2O_3$, Catal. Today 115 (2006) 191–198.
[31] C.T. Campbell, Future directions and industrial perspectives micro- and macro-kinetics: their relationship in heterogeneous catalysis, Topics Catal. 1 (1994) 353–366.
[32] D. Wolf, M. Barre-Chassonnery, M. Höhenberger, A. van Veen, M. Baerns, Kinetic study of the water gas shift reaction and its role in the conversion of methane to syngas over a Pt/MgO catalyst, Catal. Today 40 (1998) 147–156.